New high-spin isomer and quasiparticle-vibration coupling in ^{187}Ir

V. Modamio,[1,2] A. Jungclaus,[1,*] A. Algora,[3] D. Bazzacco,[4] D. Escrig,[1] L. M. Fraile,[5] S. Lenzi,[4] N. Marginean,[6] T. Martinez,[7] D. R. Napoli,[7] R. Schwengner,[8] and C. A. Ur[4,6]

[1]*Instituto de Estructura de la Materia, CSIC, Serrano 113bis, E-28006 Madrid, Spain*
[2]*Departamento de Física Teórica C-XI, Universidad Autónoma de Madrid, E-28049 Madrid, Spain*
[3]*IFIC, CSIC-Universidad Valencia, E-46071 Valencia, Spain*
[4]*Istituto Nazionale di Fisica Nucleare, Sezione di Padova, I-35131 Padova, Italy*
[5]*Universidad Complutense de Madrid, Madrid, Spain*
[6]*"Horia Hulubei" National Institute for Physics and Nuclear Engineering, Bucharest, Romania*
[7]*Istituto Nazionale di Fisica Nucleare, Laboratori Nazionali di Legnaro, I-35020 Legnaro, Italy*
[8]*Institut für Strahlenphysik, Forschungszentrum Dresden-Rossendorf, D-01314 Dresden, Germany*

(Received 16 March 2010; published 12 May 2010)

The high-spin structure of the $Z = 77$ nucleus ^{187}Ir has been studied using the fusion-evaporation reaction ^{186}W(^{7}Li,6n) at a beam energy of 59 MeV. The excitation scheme of this nucleus has been extended by more than 110 new states, including extensions of all previously established rotational bands. The band crossing region of the $h_{9/2}$ negative-parity yrast band has been revised and new intrinsic high-K states have been identified. In particular, a $29/2^-$ isomeric state [$T_{1/2} = 1.8(5)\mu$s] at an excitation energy of 2487 keV has been observed for the first time, and on top of it, a rich level scheme reaching up to spin $(59/2^-)$ and excitation energies around 7 MeV has been established.

DOI: 10.1103/PhysRevC.81.054304 PACS number(s): 23.20.Lv, 21.10.Tg, 23.20.En, 27.70.+q

I. INTRODUCTION

The osmium, iridium, and platinum ($Z = 76$–78) isotopes are located in the transitional region between the rare-earth isotopic chains of well-deformed nuclei and the semimagic lead ($Z = 82$) chain of near-spherical isotopes. In these transitional nuclei a complex interplay between different competing degrees of freedom is observed, and in particular, consideration of the γ degree of freedom plays an important role. Besides the collective excitations, a large number of different high-K multiquasiparticle states of different shapes have been observed in these nuclei. In this context, the even-even $^{186-192}$Os isotopes have been the subject of a long-standing controversy regarding the character of their low-lying excited states. In a large number of studies employing different experimental techniques such as Coulomb excitation [1–3], (p, p') and (α,α') scattering [4–7], and (^{3}H,α), (^{3}He,d), and (d,^{3}He) reactions [8–10], apparently conflicting results have been obtained, indicating, respectively, a multiphonon quadrupole, proton two-quasiparticle, and hexadecapole character of the low-lying 4_3^+ states in these nuclei. From the theoretical side, very recently the triaxial rotor model [11], the Bohr-Mottelson collective model for a soft triaxial nucleus [12], and the quasiparticle-phonon model [13] have been employed to shed light on the nature of these states; in particular, the latter study came to the conclusion that the 4_3^+ states are indeed of a mixed nature and that all experimental results can be explained naturally in a consistent way.

Given the lively debate, ongoing for many years, about the nature of the 4_3^+ states in even-even transitional Os isotopes, it seems somewhat surprising that the assignment of two-phonon $K = j + 4$ states in the odd Ir isotopes ^{187,189}Ir proposed by T. Yamazaki et al. [14] remains unappreciated. In that work a rearrangement of the states [15,16] built on the $h_{11/2}$ ($j = 11/2$) proton configuration into families with $K = j$, $K = j + 2$, and $K = j + 4$, that is, the odd $h_{11/2}$ proton coupled to the $K^\pi = 2^+$ one-phonon and the $K^\pi = 4^+$ two-phonon states in ^{186}Os, was suggested, as opposed to the standard interpretation of these states as the $h_{11/2}$ band described in the particle plus triaxial-rotor model [17,18]. The aim of the present work was, on one hand, to obtain additional information about these structures based on the $h_{11/2}$ state in ^{187}Ir and, on the other, to locate and characterize the high-spin isomer in this nucleus, whose existence has been indirectly inferred from the observation of delayed feeding into the $h_{11/2}$ band [15].

II. EXPERIMENT AND DATA PREPARATION

Excited states in ^{187}Ir were populated using the reaction ^{186}W(^{7}Li,6n) at a beam energy of 59 MeV. The beam was delivered by the XTU tandem accelerator at the Laboratori Nazionali di Legnaro and directed onto a 12 mg/cm^2 thick ^{186}W target. The γ radiation was detected in the 40 Compton-suppressed Ge detectors of the GASP array and the 80-element BGO inner ball. In addition, charged particles emitted in the $p \times n$, $d \times n$, and $t \times n$ reaction channels leading to osmium isotopes (see Refs. [19] and [20]) were detected in the Si ball ISIS consisting of 40 $\Delta E - E$ telescopes arranged in the same geometry as the Ge crystals in GASP, namely, in seven rings with $\theta = 35^\circ, 59^\circ, 72^\circ, 90^\circ, 108^\circ, 121^\circ$, and 145° with respect to the beam axis. All events with at least three coincident γ rays in the Ge detectors or two γ rays in the Ge plus one particle detected in the Si ball were recorded on tape, with the

*andrea.jungclaus@iem.cfmac.csic.es

additional condition that the γ multiplicity in the BGO ball was 3 or higher. Time distributions of γ rays were measured in a time window of 200 ns with respect to the prompt time signal of the BGO crystals. From these events, $\gamma\gamma$ matrices as well as $\gamma\gamma\gamma$ cubes were produced, both without a time condition and requiring a prompt coincidence. For the latter, two-dimensional gates on the prompt region in the energy-time matrices of all 40 Ge detectors were applied individually. The construction of the level scheme discussed in the next section is based on the $\gamma\gamma$ matrices and the $\gamma\gamma\gamma$ cubes without a particle coincidence requirement but with and without a time condition.

To determine γ-ray multipole orders, directional angular correlation ratios from oriented states (DCOs) have been measured. For this purpose, $\gamma\gamma$ events with one γ ray detected in 1 of the 12 detectors at 35° and 145° and the other detected in 1 of the 8 detectors at 72° and 108° relative to the beam direction were sorted into an asymmetric coincidence matrix. Then, using a coincidence gate on a stretched quadrupole transition γ_{gate}, the ratio R_{DCO},

$$\mathrm{R_{DCO}} = \frac{I_\gamma(\text{at } \theta_1 \,|\gamma_{\text{gate}} \text{ at } \theta_2)}{I_\gamma(\text{at } \theta_2 \,|\gamma_{\text{gate}} \text{ at } \theta_1)} \frac{\varepsilon_{\theta_2}(\gamma)\,\varepsilon_{\theta_1}(\gamma_{\text{gate}})}{\varepsilon_{\theta_1}(\gamma)\,\varepsilon_{\theta_2}(\gamma_{\text{gate}})},$$

is expected to be ≈1 for stretched quadrupole and ≈0.6 for pure dipole transitions ($\theta_1 = 35°, 145°$, $\theta_2 = 72°, 108°$). $\varepsilon_\theta(\gamma)$ are the relative efficiencies of the detectors positioned at an angle θ with respect to the beam at the energy E_γ.

III. THE LEVEL SCHEME OF ^{187}Ir

The level scheme of ^{187}Ir was established in the seventies by Kemnitz *et al.* [15] and André *et al.* [16] using (α,xn) reactions. Four rotational bands, with bandhead spins of $3/2^+$, $1/2^+$, $9/2^-$, and $11/2^-$, have been identified up to spins of $21/2^+$, $15/2^+$, $33/2^-$, and $23/2^-$, respectively. Based on the comparison with neighboring nuclei and the observed band characteristics, these bands were proposed in Refs. [15] and [16] to be built on the $3/2^+[402]$, $1/2^+[400]$, $1/2^-[541]$, and $11/2^-[505]$ proton single-particle states. The band built on the $11/2^-$ isomeric state ($T_{1/2} = 152(12)$ ns [21]) was found to be mainly fed from a state at an excitation energyof 2260 keV via a few transitions that all show delayed components. However, based on those data it was not possible to decide whether this 2260-keV state itself is long-lived or is fed from a higher-lying isomeric state via unobserved transitions. Also, no decay time could be determined for the delayed components. More recently, the $9/2^-$ band was extended up to spin $45/2^-$ employing the (^{15}N,4n) reaction and a discussion of its properties presented [22].

In the present work, the ^{186}W(^{7}Li,6n) reaction was used to populate ^{187}Ir at a high angular momentum, with the aim to localize the isomeric state and, possibly, to search for new stuctures above it. A comprehensive level scheme was established comprising 116 new excited states connected by 194 γ transitions that have been observed for the first time. Spin and parity assignments have been made mainly based on measured DCO ratios and theoretical electron conversion coefficients.

In the following sections the different parts of the excitation scheme of ^{187}Ir are discussed in detail.

A. Extension of the known bands

The established rotational bands in ^{187}Ir together with the extensions proposed in the present work are shown in Fig. 1. The ground-state band built on the $3/2^+[402]$ orbital has been extended up to spin $29/2^+$ via the observation of two additional $E2$ transitions in each of the two signatures, namely, γ rays

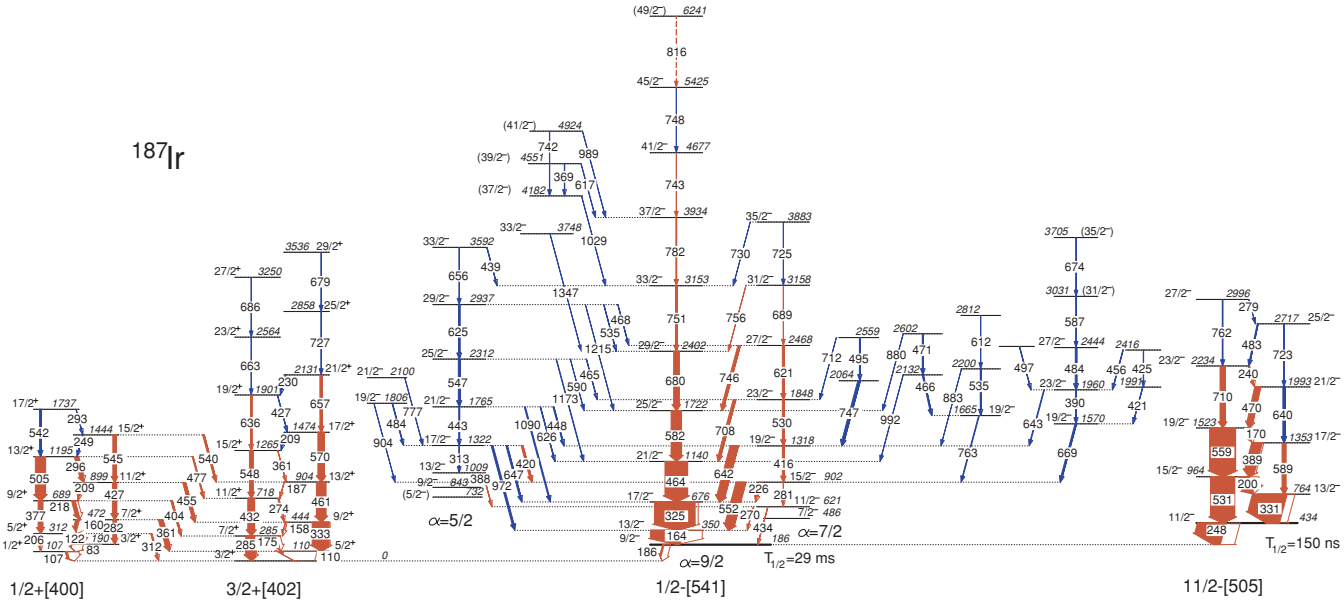

FIG. 1. (Color online) Partial level scheme (1/3) of ^{187}Ir as established in the present work. Transitions that have been observed previously [15,16,22] are shown in red, while γ rays observed for the first time in the present work are shown in blue.

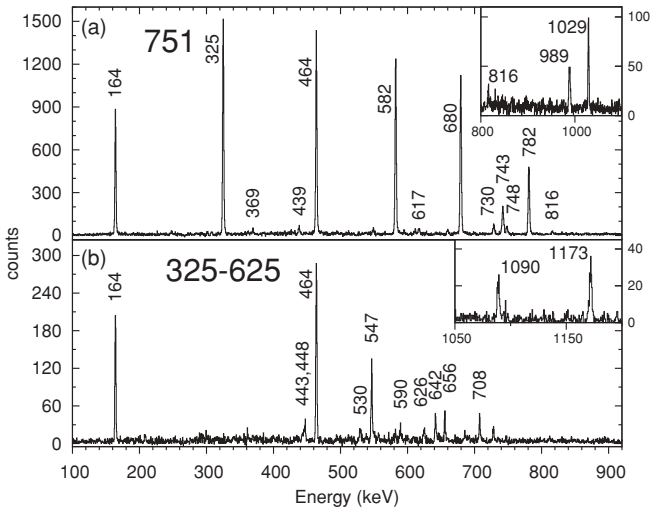

FIG. 2. (a) Double-gated coincidence spectrum with one gate on the 751-keV $33/2^- \rightarrow 29/2^-$ transition in the ($\alpha = 9/2$) $h_{9/2}$ band and the second gate on one of the in-band transitions below. (b) Double-gated coincidence spectrum with gates on the 325-keV $17/2^- \rightarrow 13/2^-$ ($\alpha = 9/2$) and 625-keV $29/2^- \rightarrow 25/2^-$ ($\alpha = 5/2$) transitions of the $h_{9/2}$ band.

of 663, 686, 727, and 679 keV. In addition, three new dipole transitions connecting states of different signatures have been observed for the first time. Only one new level with spin $17/2^+$ could be added to the $1/2^+[400]$ band decaying to the $15/2^+$ and $13/2^+$ band members.

In Ref. [15] two $\Delta I = 2$ sequences of negative parity were identified and described in the framework of the rotation-aligned coupling scheme. They are formed by an $h_{9/2}$ proton with either full or partial alignment (projections $\alpha = 9/2$ or $\alpha = 7/2$ on the rotational axis) coupled to the even-even ^{186}Os core. In the present work, we added one level with spin $35/2^-$ to the $\alpha = 7/2$ band and introduced a new $45/2^- \rightarrow 41/2^-$ transition in the negative-parity yrast band. While in Ref. [22] an 817-keV γ ray was placed to directly feed the $41/2^-$ state at 4677 keV, we propose the order of transitions in this band above the $33/2^-$ level to be 782-743-748-816 keV. This order is based on the intensities observed in the double-gated spectrum shown in Fig. 2(a), with one gate on the 751-keV $33/2^- \rightarrow 29/2^-$ and the second gate on one of the in-band transitions below. Probably, the 748-keV γ ray escaped observation in Ref. [22] owing to the multiplet structure 743-746-751-(756) keV shown in Fig. 1 of that article.

The four states at 732, 843, 1009, and 1322 keV, with spins of $(5/2^-)$, $(9/2^-)$, $(13/2^-)$, and $(17/2^-)$, respectively, were tentatively proposed to form a third, less aligned sequence with $\alpha = 5/2$ [15]. We now firmly established this band up to spin $33/2^-$ and observed a very regular decay pattern of the states of this band with spin I to the I, $I-1$, and $I-2$ members of the partner bands ($\alpha = 9/2$ and $\alpha = 7/2$) as illustrated by the coincidence spectrum with gates on the 325- and 625-keV transitions shown in Fig. 2(b).

The perturbed $h_{11/2}$ band has been established before [15,16] up to spin $23/2^-$. With the present data it was possible to extend this structure by three $E2$ and two $M1$ transitions, reaching spin $27/2^-$ and $25/2^-$ in the two signatures. Feeding into the $13/2^-$ and $17/2^-$ members of this band via transitions of 395 and 368 keV from states at 1160- and 1721-keV excitation energy, respectively, has been reported previously. New dipole sequences on top of these two states have now been established, as shown in the second part of the level scheme in Fig. 3 (see also Table I). Furthermore, a new structure has been added on top of the previously known 257 keV γ transition feeding the $23/2^-$ member of the $h_{11/2}$ band.

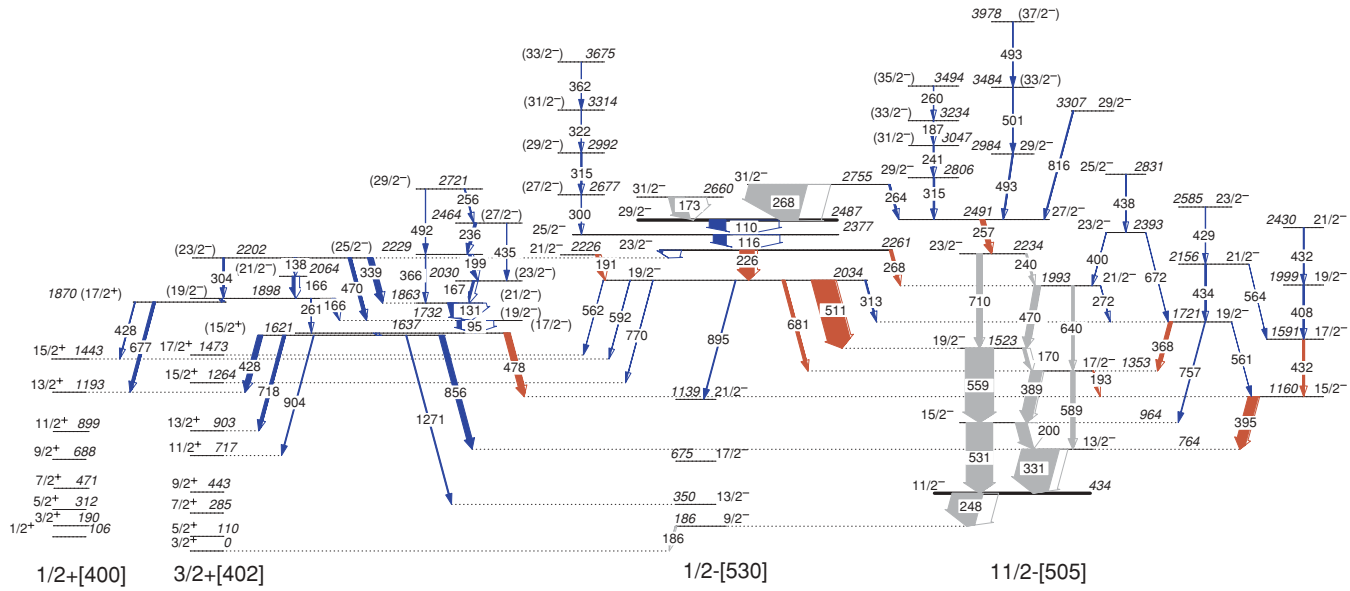

FIG. 3. (Color online) Partial level scheme (2/3) of ^{187}Ir as established in the present work. Transitions that have been observed previously [15,16,22] are shown in red, while γ rays observed for the first time in the present work are shown in blue. Some transitions belonging to the partial level schemes (1/3) and (3/3) are included here, in gray, to facilitate the readability of the figures.

TABLE I. Energies, intensities, R_{DCO} ratios, initial- and final-state spins, and initial-state excitation energies of γ rays included in the partial level schemes of ^{187}Ir shown in Figs. 1 and 3. Intensities are not corrected for internal conversion.

E_γ (keV)	I_γ	R_{DCO}	I_i^π	I_f^π	E_i (keV)
16.2			$(17/2)^-$	$(15/2)^+$	1637
28.0			$(19/2)^-$	$(17/2)^+$	1898
59.2			$23/2^-$	$(23/2)^-$	2261
82.61	33(8)		$3/2^+$	$1/2^+$	190
94.8	131(6)		$(19/2)^-$	$(17/2)^-$	1732
106.8	68(4)	1.4(2)	$1/2^+$	$3/2^+$	107
109.8	500(20)	1.08(09)	$29/2^-$	$25/2^-$	2487
110.2	619(182)	0.98(09)	$5/2^+$	$3/2^+$	110
116.3	392(6)	1.02(10)	$25/2^-$	$23/2^-$	2377
122.4	62(6)	0.9(3)	$5/2^+$	$3/2^+$	312
131.0	287(9)		$(21/2)^-$	$(19/2)^-$	1863
138.3	23(4)	1.0(2)	$(23/2)^-$	$(21/2)^-$	2202
157.9	25(2)		$9/2^+$	$7/2^+$	444
159.7	60(5)	0.78(15)	$7/2^+$	$5/2^+$	472
164.2	1000(10)	0.87(3)	$13/2^-$	$9/2^-$	350
165.9	42(11)		$(19/2)^-$	$(19/2)^-$	1898
166.2	65(5)	0.63(17)	$(21/2)^-$	$(19/2)^-$	2064
166.6	90(20)		$(23/2)^-$	$(21/2)^-$	2030
170.4	95(5)	0.72(9)	$19/2^-$	$17/2^-$	1523
175.4	91(2)	0.54(09)	$7/2^+$	$5/2^+$	285
186.2			$9/2^-$	$3/2^-$	186
186.6	5(2)		$13/2^+$	$11/2^+$	904
186.8	10(2)		$(33/2)^-$	$(31/2)^-$	3234
191.4	82(3)	0.86(8)	$21/2^-$	$19/2^-$	2225
193.1	15(2)		$17/2^-$	$15/2^-$	1353
199.3	76(16)		$(25/2)^-$	$(23/2)^-$	2229
200.0	341(8)	0.80(4)	$15/2^-$	$13/2^-$	964
205.6	22(3)		$5/2^+$	$1/2^+$	312
209.0			$17/2^+$	$15/2^+$	1474
209.2	23(10)		$11/2^+$	$9/2^+$	899
217.6	119(17)	0.80(8)	$9/2^+$	$7/2^+$	689
226.3	42(1)	0.86(12)	$15/2^-$	$17/2^-$	902
226.4	431(7)	0.98(6)	$23/2^-$	$19/2^-$	2261
230.4			$21/2^+$	$19/2^+$	2131
235.9	52(12)		$(27/2)^-$	$(25/2)^-$	2464
241.0	21(3)	0.80(13)	$(31/2)^-$	$29/2^-$	3047
241.0	36(3)	0.74(15)	$23/2^-$	$21/2^-$	2234
247.8	907(10)	0.64(12)	$11/2^-$	$9/2^-$	434
249.4	9(2)		$15/2^+$	$13/2^+$	1444
256.4	22(6)		$(29/2)^-$	$(27/2)^-$	2721
257.0	127(3)	0.92(5)	$27/2^-$	$23/2^-$	2491
260.5	8(1)		$(35/2)^-$	$(33/2)^-$	3494
260.6	68(12)		$(19/2)^-$	$(17/2)^-$	1898
263.6	44(4)	1.04(10)	$31/2^-$	$27/2^-$	2755
268.1	66(12)		$23/2^-$	$21/2^-$	2261
270.2	1(1)		$11/2^-$	$13/2^-$	621
272.1	8(2)		$21/2^-$	$19/2^-$	1993
274.2	29(6)	0.64(09)	$11/2^+$	$9/2^+$	718
279.8			$27/2^-$	$25/2^-$	2996
281.3	1(1)		$15/2^-$	$11/2^-$	902
282.0	102(7)	0.74(4)	$7/2^+$	$3/2^+$	472
285.4	324(34)	1.02(10)	$7/2^+$	$3/2^+$	285
293.7	5(1)		$17/2^+$	$15/2^+$	1737
295.9	112(35)	0.88(16)	$13/2^+$	$11/2^+$	1195
299.8	54(7)		$(27/2)^-$	$25/2^-$	2677
304.2	37(4)		$(23/2)^-$	$(19/2)^-$	2202
311.9	34(6)	0.63(6)	$5/2^+$	$3/2^+$	312
313.2	1(1)		$17/2^-$	$13/2^-$	1322
313.4	32(2)	1.2(2)	$19/2^-$	$19/2^-$	2034
314.6	37(4)	0.84(10)	$29/2^-$	$27/2^-$	2806
314.9	23(11)		$(29/2)^-$	$(27/2)^-$	2992
322.1	8(4)		$(31/2)^-$	$(29/2)^-$	3314
325.0	1332(17)	1.11(2)	$17/2^-$	$13/2^-$	675
330.6	1101(12)	0.92(3)	$13/2^-$	$11/2^-$	764
333.1	551(7)	0.98(07)	$9/2^+$	$5/2^+$	444
338.9	140(20)	0.51(14)	$(23/2)^-$	$(21/2)^-$	2202
360.9	21(3)		$15/2^+$	$13/2^+$	1265
361.2	136(4)	0.91(10)	$7/2^+$	$5/2^+$	472
361.6	6(3)		$(33/2)^-$	$(31/2)^-$	3675
365.6			$(25/2)^-$	$(21/2)^-$	2229
368.3	100(3)	1.21(17)	$19/2^-$	$17/2^-$	1721
369.4	1(1)		$(39/2^-)$	$(37/2^-)$	4551
377.1	148(22)	0.99(5)	$9/2^+$	$5/2^+$	689
388.4	1(1)		$13/2^-$	$11/2^-$	1009
388.6	338(12)	0.95(5)	$17/2^-$	$15/2^-$	1353
389.7	24(1)		$23/2^-$	$19/2^-$	1960
392.7	2(1)		$25/2^-$	$21/2^-$	2413
395.4	294(6)	0.94(7)	$15/2^-$	$13/2^-$	1160
400.3	13(3)	0.9(2)	$23/2^-$	$21/2^-$	2393
403.8	51(5)	0.55(10)	$9/2^+$	$7/2^+$	689
407.6	39(2)		$19/2^-$	$17/2^-$	1999
415.8	62(2)	1.08(19)	$19/2^-$	$15/2^-$	1318
420.4	59(2)	0.69(12)	$17/2^-$	$15/2^-$	1322
421.4	6(1)			$19/2^-$	1991
424.6	2(1)				2416
426.7	138(34)		$11/2^+$	$7/2^+$	899
427.3			$19/2^+$	$17/2^+$	1900
427.9	140(10)	1.01(7)	$(15/2^+)$	$13/2^+$	1621
428.0	23(5)		$(17/2^+)$	$15/2^+$	1870
429.2			$23/2^-$	$21/2^-$	2585
431.4	58(1)		$17/2^-$	$15/2^-$	1591
			$21/2^-$	$19/2^-$	2430
432.1	219(22)	0.97(05)	$11/2^+$	$7/2^+$	718
434.4	1(1)		$11/2^-$	$9/2^-$	621
434.4	35(5)	0.7(3)	$21/2^-$	$19/2^-$	2156
434.7			$(27/2^-)$	$(23/2^-)$	2464
437.7	6(2)		$25/2^-$	$23/2^-$	2831
438.8	1(1)		$33/2^-$	$33/2^-$	3592
443.4	29(1)	1.4(4)	$21/2^-$	$17/2^-$	1765
447.8	29(1)	0.50(14)	$21/2^-$	$19/2^-$	1765
455.0	93(19)	0.75(11)	$11/2^+$	$9/2^+$	899
455.8	14(3)			$23/2^-$	2416
460.6	305(63)	0.96(09)	$13/2^+$	$9/2^+$	904
464.2	722(16)	1.01(3)	$21/2^-$	$17/2^-$	1140
464.6	18(5)		$25/2^-$	$23/2^-$	2312
466.3	38(2)		$23/2^-$	$19/2^-$	2132
468.3	1(1)		$29/2^-$	$27/2^-$	2937
469.9	184(4)	0.56(9)	$21/2^-$	$19/2^-$	1993
470.1	95(12)	0.76(14)	$(23/2)^-$	$(19/2)^-$	2202
470.8	35(2)				2602
477.0	32(9)		$13/2^+$	$11/2^+$	1195

TABLE I. (*Continued*.)

E_γ (keV)	I_γ	R_{DCO}	I_i^π	I_f^π	E_i (keV)
477.6	173(3)		$(17/2)^-$	$15/2^-$	1637
482.6	34(10)		$25/2^-$	$23/2^-$	2717
483.8	17(5)		$19/2^-$	$17/2^-$	1806
484.1	50(2)	1.04(11)	$27/2^-$	$23/2^-$	2444
492.0			$(29/2^-)$	$(25/2^-)$	2721
492.4	52(2)	1.03(11)	$29/2^-$	$27/2^-$	2984
492.9			$(37/2)^-$	$(33/2)^-$	3978
494.7	27(5)				2559
497.3	11(2)		$25/2^-$	$23/2^-$	2458
500.7	17(2)		$(33/2)^-$	$29/2^-$	3484
505.2	329(99)	1.03(12)	$13/2^+$	$9/2^+$	1195
511.1	681(14)	1.01(3)	$19/2^-$	$19/2^-$	2034
529.9	65(2)	1.3(5)	$23/2^-$	$19/2^-$	1848
530.6	781(13)	0.97(4)	$15/2^-$	$11/2^-$	964
535.0	1(1)		$29/2^-$	$29/2^-$	2937
535.2	28(1)	0.8(3)	$23/2^-$	$19/2^-$	2200
539.8	53(5)		$15/2^+$	$13/2^+$	1444
542.2	59(7)	0.89(9)	$17/2^+$	$13/2^+$	1737
545.1	112(35)	1.0(2)	$15/2^+$	$11/2^+$	1444
546.8	56(2)	0.97(7)	$25/2^-$	$21/2^-$	2312
547.6	114(28)	0.98(08)	$15/2^+$	$11/2^+$	1265
551.5	305(7)	0.46(3)	$15/2^-$	$13/2^-$	902
559.0	837(14)	0.98(4)	$19/2^-$	$15/2^-$	1523
561.4			$19/2^-$	$15/2^-$	1721
561.6	51(4)	0.88(11)	$19/2^-$	$17/2^+$	2034
564.4			$21/2^-$	$17/2^-$	2156
569.6	209(10)	1.00(06)	$17/2^+$	$13/2^+$	1474
582.5	337(8)	1.05(3)	$25/2^-$	$21/2^-$	1722
586.7	12(2)		$(31/2^-)$	$27/2^-$	3031
588.6	123(4)		$17/2^-$	$13/2^-$	1353
589.7	6(1)		$25/2^-$	$25/2^-$	2312
591.6	42(9)		$19/2^-$	$15/2^+$	2034
611.9	5(2)				2812
617.3	2(1)		$(39/2^-)$	$37/2^-$	4551
621.1	64(2)	1.07(14)	$27/2^-$	$23/2^-$	2468
624.7	45(2)	0.67(9)	$29/2^-$	$25/2^-$	2937
625.6	17(2)	1.04(19)	$21/2^-$	$21/2^-$	1765
636.1	47(12)	0.73(14)	$19/2^+$	$15/2^+$	1900
640.2	69(2)		$21/2^-$	$17/2^-$	1993
642.2	261(18)	0.50(2)	$19/2^-$	$17/2^-$	1318
642.8	23(6)	1.0(2)	$23/2^-$	$19/2^-$	1960
646.8	44(1)	0.88(6)	$17/2^-$	$17/2^-$	1322
655.6	16(4)	1.42(16)	$33/2^-$	$29/2^-$	3592
657.0	81(8)	1.06(13)	$21/2^+$	$17/2^+$	2131
662.7	7(2)		$23/2^+$	$19/2^+$	2564
668.6	51(2)	0.75(14)	$19/2^-$	$15/2^-$	1570
672.2	15(2)		$23/2^-$	$19/2^-$	2393
674.1	6(2)		$(35/2^-)$	$(33/2^-)$	3705
677.0	84(1)	0.96(14)	$(17/2^+)$	$13/2^+$	1870
678.6	11(3)		$29/2^+$	$25/2^+$	3536
679.7	173(8)	1.02(6)	$29/2^-$	$25/2^-$	2402
681.5	89(3)	0.74(9)	$19/2^-$	$17/2^-$	2034
685.8	6(2)		$27/2^+$	$23/2^+$	3250
689.4	10(1)		$31/2^-$	$27/2^-$	3158
707.8	88(2)	0.40(3)	$23/2^-$	$21/2^-$	1848
710.4	167(3)	0.99(6)	$23/2^-$	$19/2^-$	2234
711.5	9(1)			$23/2^-$	2559

TABLE I. (*Continued*.)

E_γ (keV)	I_γ	R_{DCO}	I_i^π	I_f^π	E_i (keV)
718.0	91(3)	1.11(10)	$(15/2^+)$	$13/2^+$	1621
723.3	13(2)		$25/2^-$	$21/2^-$	2717
724.8	8(1)		$35/2^-$	$31/2^-$	3883
726.6	16(3)		$25/2^+$	$21/2^+$	2858
730.0	3(1)		$35/2^-$	$33/2^-$	3883
742.6	8(1)		$(41/2^-)$	$(37/2^-)$	4677
746.4	80(30)	0.36(2)	$27/2^-$	$25/2^-$	2468
746.7	46(1)			$19/2^-$	2064
748.2	3(1)		$45/2^-$	$41/2^-$	5425
751.2	56(1)	0.83(6)	$33/2^-$	$29/2^-$	3153
756.3	10(1)		$31/2^-$	$29/2^-$	3158
756.8	23(1)	1.1(4)	$19/2^-$	$15/2^-$	1721
762.2	24(2)	1.1(2)	$27/2^-$	$23/2^-$	2996
763.4	23(1)		$19/2^-$	$15/2^-$	1665
769.8	14(4)	1.5(5)	$19/2^-$	$15/2^+$	2034
777.4	17(1)		$21/2^-$	$17/2^-$	2100
781.6	28(1)	0.53(15)	$37/2^-$	$33/2^-$	3934
815.6	2(1)		$(49/2^-)$	$45/2^-$	6241
816.2	31(4)	0.9(2)	$29/2^-$	$27/2^-$	3307
856.8	161(9)		$(15/2)^+$	$13/2^-$	1621
880.4	4(1)			$25/2^-$	2602
882.7	5(1)			$19/2^-$	2200
894.7	27(1)		$19/2^-$	$21/2^-$	2034
903.6	10(1)		$19/2^-$	$15/2^-$	1806
904.3	28(8)	0.85(17)	$(15/2^+)$	$11/2^+$	1621
971.5	61(3)	0.92(18)	$17/2^-$	$13/2^-$	1322
989.0	3(1)		$(41/2^-)$	$37/2^-$	4924
991.5	16(2)			$21/2^-$	2132
1029.0	5(1)		$(37/2^-)$	$33/2^-$	4182
1089.5	37(2)	1.06(15)	$21/2^-$	$17/2^-$	1765
1173.0	18(2)		$25/2^-$	$21/2^-$	2312
1214.7	1(1)		$29/2^-$	$25/2^-$	2937
1270.9	33(2)		$(15/2^+)$	$13/2^-$	1621
1272.9	9(1)		$25/2^-$	$21/2^-$	2413
1346.6	1(1)		$33/2^-$	$29/2^-$	3748

B. New high-spin structures and an $I^\pi = 29/2^-$ high-spin isomer at 2487 keV

In the coincidence spectrum with a gate on the 478-keV transition, which was placed in Refs. [15] and [16] as populating the 1160-keV level mentioned before from a state at an excitation energy of 1637 keV, a large number of lines with a relatively low intensity are observed. In double coincidence with, in each case, two of these lines, the low-lying γ transitions of all four known rotational bands are clearly visible. Careful analysis of all coincidence relations identified the five γ rays with energies of 428, 718, 856, 904, and 1271 keV as the ones connecting the newly observed transitions above the 1637-keV level to the four known rotational bands. However, proper summing of energies indicates the existence of a new state at 1621 keV that must be populated from the 1637-keV level via an unobserved 16-keV transition (see Fig. 3).

Besides the 395- and 368-keV γ rays populating the $h_{11/2}$ band mentioned before, a few more feeding transitions were

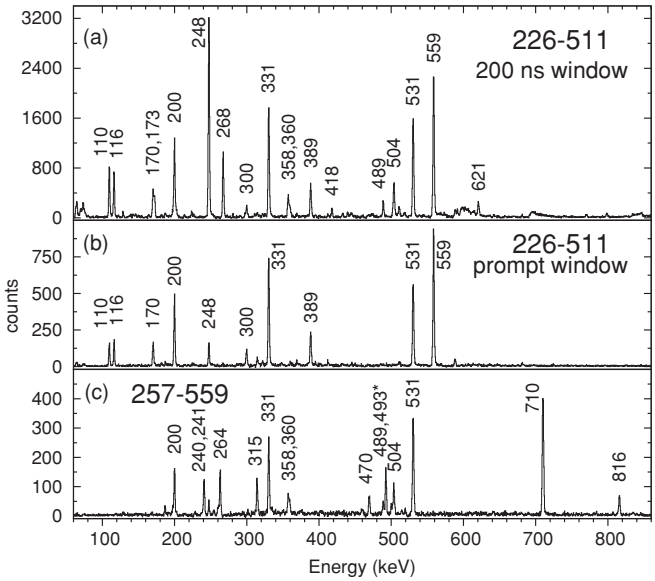

FIG. 4. Double-gated coincidence spectra with gates on the 226- and 511-keV transitions: (a) without a time condition and (b) with a prompt time window. (c) Double-gated coincidence spectrum with a gate on the 257- and 559-keV transitions.

identified in Refs. [15] and [16], namely, the 511- and 681-keV γ rays decaying from a 2034-keV, $19/2^-$ state and the 191- and 226-keV transitions feeding this state. It was noted that all these transitions have a delayed component, indicating the existence of an isomeric state in this region of the level scheme [15]. In the present work it has been possible to unequivocally identify the position of this isomer and to establish its decay pattern. In the first step double-gated coincidence spectra with gates on the 511- and 226-keV γ rays were created, both requiring a prompt coincidence in time and not applying a time condition. In the latter case the full hardware coincidence time window of about 200 ns was used. The two resulting spectra are compared in Figs. 4(a) and 4(b). In the prompt spectrum, in addition to the known transitions of the $h_{11/2}$ band below the $19/2^-$ state as well as the 248-keV transition corresponding to the decay of the $h_{11/2}$ band head with a half-life of $T_{1/2} = 152$ ns [21], only three new lines, at 110, 116, and 300 keV, are clearly visible and have been placed, according to their mutual coincidence relations, on top of the 2261-keV state. In the spectrum without a time condition, however, a number of additional new lines, with energies of 173, 268, 358, 360, 418, 489, 504, and 621 keV, appear. The disappearance of these lines in the prompt spectrum indicates a long lifetime of the level at 2487 keV. This isomeric state is populated by the parallel 173- and 268-keV lines, which in turn have been the starting point for the construction of the level scheme on top of the isomer using prompt coincidences that are presented in Sec. III C. The position of the isomeric state is unambiguously fixed by the observation of a weak prompt branch connecting the newly established 2755-keV state above the isomer to the $23/2^-$ member of the $h_{11/2}$ band via two γ transitions of 264 and 257 keV (see Fig. 3). This prompt path is illustrated by the double-coincidence spectrum with gates on the 257- and 559-keV transitions in Fig. 4(c), in which most of the new lines identified in Fig. 4(a) are visible too, namely, those of 358, 360, 489, and 504 keV. In addition, two new sequences of γ rays, 315-241-187-260 and 493-501-493 keV, have been observed and placed on top of the 2491-keV state (compare Fig. 3). With respect to the spins of the newly established states, the levels at 2491 and 2755 keV have been assigned spins of $27/2^-$ and $31/2^-$ based on the DCO ratios of 0.92(5) and 1.04(10) of the 257- and 264-keV transitions, respectively, suggesting them to be of $E2$ character. The tentative assignment of spin $23/2^-$ to the 2261-keV state [15] is confirmed by our DCO information. For the isomeric state at 2487 keV a spin of $29/2^-$ is proposed based on the DCO ratio of 0.73(2) for the 268-keV γ ray feeding this state from the 2755-keV, $31/2^-$ level. The spin of the 2377-keV level has been decided on based on the observed intensities of the 110- and 116-keV transitions. In a double-coincidence spectrum with gates on the 268-keV transition above and the 559-keV γ ray below the 110- to 116-keV cascade, the observed relative intensities of these two low-energy transitions depend only on their conversion coefficients. A comparison of the experimental intensity ratio $I(110\text{ keV})/I(116\text{ keV}) = [1 + \alpha(116\text{ keV})]/[1 + \alpha(110\text{ keV})] = 1.27(10)$ with the conversion coefficient α to the corresponding theoretical ratios assuming multipolarities $E1$, $M1$, $E2$, and $M2$ for each of the two transitions leads to the conclusion that only the combination of the $E2$ character of the 110-keV with $M1$ character of the 116-keV transition results in a value, namely, 1.23, in agreement with the experimental result. Because this solution is also consistent with the spin difference $\Delta I = 3\hbar$ between the $23/2^-$ state at 2261 keV and the $29/2^-$ level at 2487 keV, we propose a spin/parity of $25/2^-$ for the 2377-keV state.

1. The lifetime of the 2487-keV, $I^\pi = 29/2^-$ isomer

Within the hardware coincidence time window of about 200 ns used in this experiment, the time spectra of the transitions below the $29/2^-$ isomer are constant within the statistical uncertainties, indicating that the isomeric lifetime is large compared to the observed time range and therefore not directly measurable under the present experimental conditions. To get at least an estimate of it, we compared the γ-ray multiplicity distributions obtained for transitions above and below the isomeric state. Figure 5 shows the multiplicities of the γ-ray cascades observed in the BGO inner ball in coincidence with the 268-keV, $31/2^- \rightarrow 29/2^-$ transition directly above and the 226-keV, $23/2^- \rightarrow 19/2^-$ transition below the isomeric state. The distribution belonging to the 268-keV transition shows only one component corresponding to the average multiplicity of γ rays between the entry region after the fusion-evaporation reaction and the $31/2^-$ state (of course, modified by the finite detection efficiency of the BGO ball). The distribution in coincidence with the 226-keV transition, on the contrary, is clearly composed of two different components. The one with the larger average multiplicity corresponds to the cascades in which the isomeric state decayed during the 200-ns time window, and the one

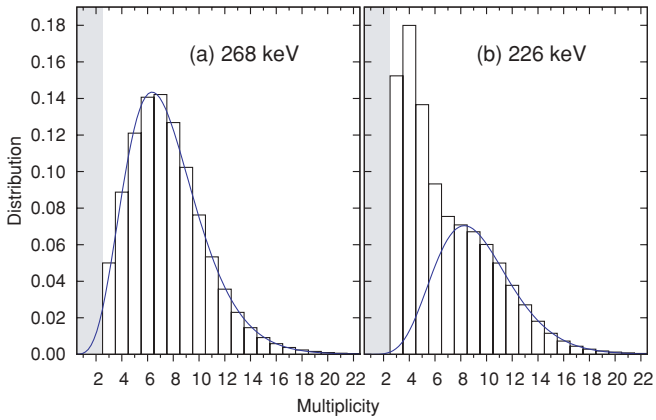

FIG. 5. (Color online) Multiplicity of the γ-ray cascade observed in the BGO array in coincidence with (a) the 268-keV, $31/2^- \rightarrow 29/2^-$ transition above and (b) the 226-keV, $23/2^- \rightarrow 19/2^-$ transition below the isomeric $I^\pi = 29/2^-$ state. The solid (blue) curves represent fits according to Eq. (1).

peaking at low multiplicity comprises the events in which the γ rays from the decay of the isomer once again triggered the data acquisition. The relative weight of these two components depends on the ratio between the lifetime of the state and the considered time window. For an infinite lifetime the two components would have equal weight.

In the case of the 268-keV transition the multiplicity distribution can be described by a Γ distribution,

$$G_{(k,\theta)}(x) = x^{k-1}\frac{\exp(-x/\theta)}{\theta^k \times \Gamma(k)}, \tag{1}$$

with the form parameter k and the scale parameter θ. The higher-multiplicity component of the observed multiplicity distribution in coincidence with the 226-keV transition can be approximated by the same function, Eq. (1), including a normalization factor $\beta = 0.519(6)$ [cf. Fig. 5(b)]. The fraction of nuclei for which the isomeric state does not decay within the time window of $\Delta T = 200$ ns, and which therefore contributes to the low-multiplicity component, is given by

$$\chi = \left(\frac{1-\beta}{\beta}\right) = \frac{N}{N_0} = \exp(-\Delta T/\tau). \tag{2}$$

Using this approach the half-life of the 2487-keV, $I^\pi = 29/2^-$ isomeric state is estimated as $T_{1/2} = 1.8(5)\ \mu$s.

C. Structures above the $I^\pi = 29/2^-$ isomer

While no transitions above the $29/2^-$ isomeric state have been observed in previous experimental studies, the γ ray of 268 keV populating this state is the dominant line in the total projection of the $\gamma\gamma$ matrices obtained in the present experiment (cf. Fig. 1(a) of Ref. [19]). Starting from the coincidence spectrum with a gate on this transition, a comprehensive excitation scheme has been established above the isomer reaching up to spin $(59/2^-)$. The main sequence is illustrated in Fig. 6(a), which shows the double-gated coincidence spectrum with gates on the 504- and 890-keV transitions. It consists of two irregular $E2$ cascades,

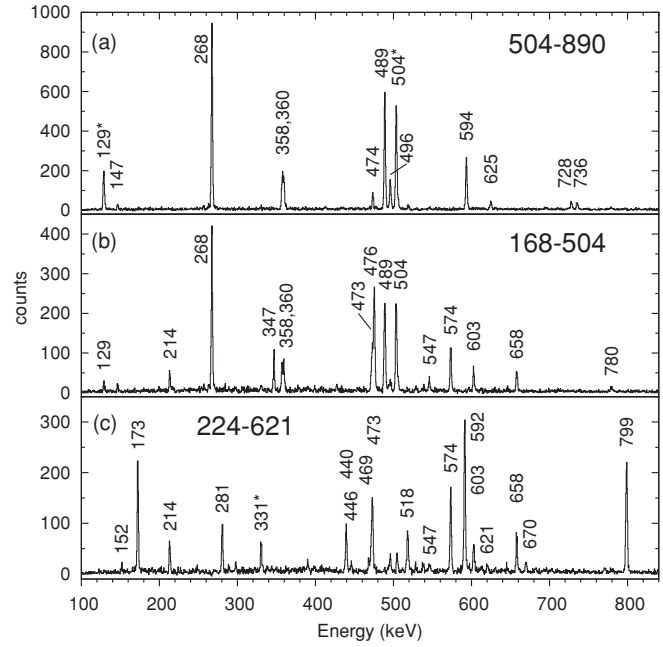

FIG. 6. Double-gated coincidence spectra with gates on the (a) 504- and 890-keV transitions, (b) the 168- and 504-keV transitions, and (c) the 224- and 621-keV transitions of the excitation scheme built on the 2487-keV, $29/2^-$ isomeric state. Lines marked with an asterisk are doublets.

504-489-740 and 506-563 keV, with strong connecting $M1$ transitions. An additional $E2$ cascade, 460-520-743 keV, decays into the $33/2^-$ member of the main sequence via a γ ray of 358 keV. The construction of this part of the excitation scheme, shown in Fig. 7 (see also Table II), was hampered by the existence of a number of doublets, namely, at energies of 129, 358, and 504 keV.

Besides the structure on top of the 268-keV transition discussed above, a second intense sequence was observed based on the 173-keV γ ray populating the isomeric state in parallel to the 268-keV branch. The spin of the 2660-keV level has been deduced on the basis of DCO and intensity information. The DCO ratio of 0.58(2) for the 173-keV transition indicates $\Delta I = 1$. In addition, the relative intensities of the 173- and 418-keV lines observed in a double-gated coincidence spectrum with gates on the 592- and 203-keV transitions above can only be explained assuming a $M1$ character ($\alpha_{M1} = 1.33$, $\alpha_{E1} = 0.099$) for the 173-keV γ ray. We therefore propose a spin of $31/2^-$ for the 2660-keV state. On top of this state we again observe two sequences of $E2$ transitions, 621-592-799 and 643-670 keV, with strong $M1$ transitions connecting them. Interestingly, the structures built on the two $31/2^-$ states at 2660 and 2755 keV, respectively, are interconnected at a higher angular momentum. Both the 4896-keV, $47/2^-$ and the 6241-keV, $57/2^-$ states have decay branches to both structures, via the 224- and 168-keV γ rays in the first case and the 214- and 474-keV transitions in the latter. As an illustration, the double-gated coincidence spectra with gates on the 168- and 504-keV with respect to the 224- and 621-keV transitions are shown in Figs. 6(b)

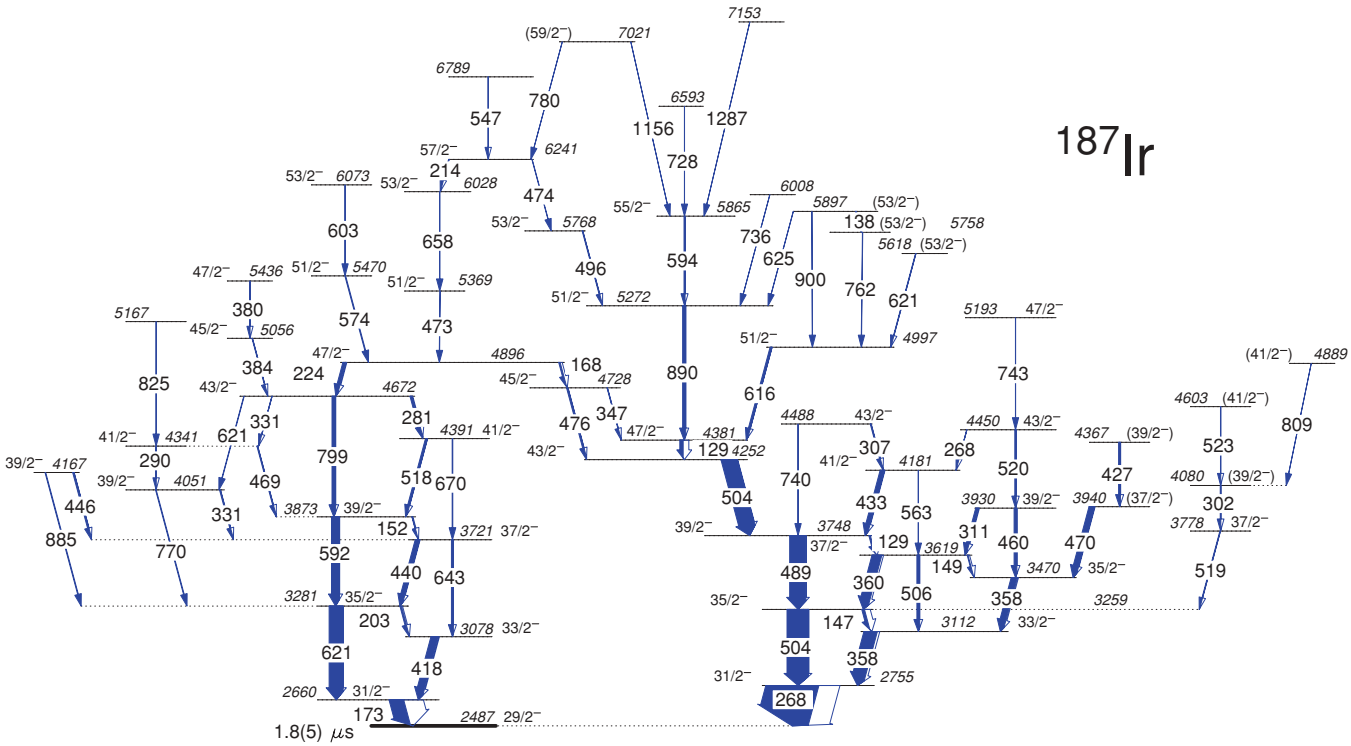

FIG. 7. (Color online) Partial level scheme (3/3) of ^{187}Ir as established in the present work showing the stuctures above the $I^{\pi} = 29/2^{-}$ high-spin isomer at 2487 keV. All γ rays included in this scheme were observed for the first time in the present work.

and 6(c). In both spectra, lines of 214, 473, 547, 574, 603, and 658 keV corresponding to transitions placed above the 4896-keV, $47/2^{-}$ state are clearly visible.

IV. DISCUSSION

In this section several aspects of the comprehensive level scheme of ^{187}Ir are discussed in more detail, namely, the backbending observed in the rotation-aligned $h_{9/2}$ band, the structure of the observed multiquasiparticle states, and the coupling between γ vibrations and quasiparticle excitations as first proposed by Yamazaki *et al.* [14].

A. Backbending in the rotation-aligned $h_{9/2}$ band

The origin of the first band crossings observed in the $A = 170$–190 mass region has been the subject of numerous experimental and theoretical studies in the past. However, to date no clear and consistent picture has been obtained. In general, in this mass region, the first band crossing is caused by the rotational alignment of either a pair of $h_{9/2}$ quasiprotons or a pair of $i_{13/2}$ quasineutrons. Odd-Z Ir isotopes are of particular interest in this context because, for the low-lying $h_{9/2}$ bands in these isotopes, the first quasiproton crossing is blocked. An abrupt change in the frequency of the first crossing has been observed between ^{181,183}Ir ($N = 104, 106$) and ^{185}Ir ($N = 108$) for a long time. Different explanations for this behavior have been proposed: In Ref. [23], it was concluded that while in the lighter isotopes ($N \leqslant 106$) a $(\nu i_{13/2})^2$ alignment is observed at a frequency of about $\hbar\omega = 0.29$ MeV, two $h_{9/2}$ protons are responsible for the crossing in ^{185}Ir at the significantly higher frequency of $\hbar\omega = 0.39$ MeV.

In a very systematic study of the alignment process in a number of isotopes in this region [24], on the contrary, it was discussed that an $i_{13/2}$ quasineutron alignment could be responsible for the crossing in all three cases, $N = 104$, 106, and 108, with the variation in crossing frequency being caused by shape changes. More recently the $h_{9/2}$ band in ^{187}Ir was observed up to spin $(45/2^{-})$ [22], showing a band crossing at the same frequency as the one observed in ^{185}Ir. Furthermore, it was found in that work that the alignment gain in ^{185,187}Ir is $2\hbar$ smaller compared to those in the lighter isotopes. In particular, the latter observation was considered an additional argument in favor of the interpretation given in Ref. [23], namely, the assignment of a blocked proton $h_{9/2}$ band crossing in ^{185,187}Ir. As discussed in Sec. III A, our new experimental information led to a revision of the high-spin part of the $h_{9/2}$ band in ^{187}Ir. The resulting modified aligned angular momentum plot is shown in Fig. 8(a). With the newly established sequence (see Fig. 1), the alignment gain in ^{187}Ir is now the same (about $7\hbar$) as the one observed in ^{181,183}Ir, which contradicts the argument given by Danchev *et al.* [22]. In Fig. 8(b) we show for comparison the aligned angular momenta for the ground-state bands in the even-even $N = 106$–110 core nuclei $^{182-186}$Os. In these nuclei a corresponding shift in crossing frequency is observed between the $N = 106$ isotope ^{182}Os (isotone of ^{183}Ir) and the $N = 108$, 110 isotopes ^{184,186}Os (isotones of ^{185,187}Ir), ruling out blocking effects as the main reason for the observed shift in crossing frequencies along the Ir isotopic chain.

TABLE II. Energies, intensities, R_{DCO} ratios, initial- and final-state spins, and initial-state excitation energies of γ rays included in the partial level scheme of ^{187}Ir shown in Fig. 7. Intensities are not corrected for internal conversion.

$E\gamma$ (keV)	I_γ	R_{DCO}	I_i^π	I_f^π	E_i (keV)
128.8	111(5)	0.98(4)	$47/2^-$	$43/2^-$	4381
129.4	50(15)		$39/2^-$	$37/2^-$	3748
138.4	1(1)			$(53/2)^-$	5897
146.7	87(3)	0.65(5)	$35/2^-$	$33/2^-$	3259
149.0	25(7)		$37/2^-$	$35/2^-$	3619
152.1	12(1)		$39/2^-$	$37/2^-$	3873
168.4	46(1)	0.58(4)	$47/2^-$	$45/2^-$	4896
172.6	470(35)	0.58(2)	$31/2^-$	$29/2^-$	2660
203.0	44(6)	0.78(12)	$35/2^-$	$33/2^-$	3281
213.6	15(2)	0.86(8)	$57/2^-$	$53/2^-$	6241
224.0	102(9)	0.97(6)	$47/2^-$	$43/2^-$	4896
267.5	1700(30)	0.73(2)	$31/2^-$	$29/2^-$	2755
268.0			$43/2^-$	$41/2^-$	4450
281.0	66(6)	0.81(5)	$43/2^-$	$41/2^-$	4672
289.6	10(1)		$41/2^-$	$39/2^-$	4341
302.0	64(7)		$(39/2)^-$	$37/2^-$	4080
306.7	25(2)	0.70(14)	$43/2^-$	$41/2^-$	4488
311.1	94(3)	0.85(8)	$39/2^-$	$37/2^-$	3930
330.7	27(3)	0.87(15)	$43/2^-$	$41/2^-$	4051
			$39/2^-$	$37/2^-$	4672
346.8	13(2)	0.74(14)	$45/2^-$	$47/2^-$	4728
357.4	197(8)		$35/2^-$	$33/2^-$	3470
357.6	430(50)	0.93(3)	$33/2^-$	$31/2^-$	3112
359.6	315(8)	0.87(3)	$37/2^-$	$35/2^-$	3619
380.1	4(1)	0.67(5)	$47/2^-$	$45/2^-$	5436
383.7	15(2)	0.62(5)	$45/2^-$	$43/2^-$	5056
418.2	240(20)	1.07(10)	$33/2^-$	$31/2^-$	3078
426.9	61(12)		$(39/2)^-$	$(37/2)^-$	4367
432.9	141(4)	0.87(6)	$41/2^-$	$39/2^-$	4181
439.8	142(13)	0.98(7)	$37/2^-$	$35/2^-$	3721
446.2	43(4)	0.71(16)	$39/2^-$	$37/2^-$	4167
460.3	92(3)		$39/2^-$	$35/2^-$	3930
468.8	25(3)	0.89(10)	$41/2^-$	$39/2^-$	4341
469.9	180(7)		$(37/2)^-$	$35/2^-$	3940
473.0	22(3)	0.91(4)	$51/2^-$	$47/2^-$	5369
473.6	10(1)	0.9(5)	$57/2^-$	$53/2^-$	6241
475.6	65(6)	0.62(8)	$45/2^-$	$43/2^-$	4728
489.2	540(40)	1.02(3)	$39/2^-$	$35/2^-$	3748
496.3	20(3)	0.67(6)	$53/2^-$	$51/2^-$	5768
503.5	525(25)	0.94(5)	$43/2^-$	$39/2^-$	4252
504.1	700(100)	0.96(3)	$35/2^-$	$31/2^-$	3259
506.1	91(5)		$37/2^-$	$33/2^-$	3617
518.4	64(7)	1.27(13)	$41/2^-$	$39/2^-$	4391
519.4	128(3)	0.78(9)	$37/2^-$	$35/2^-$	3778
519.8	46(2)		$43/2^-$	$39/2^-$	4450
522.6	19(4)		$(41/2)^-$	$(39/2)^-$	4603
547.4	10(2)			$57/2^-$	6789
563.4	11(3)		$41/2^-$	$37/2^-$	4181
573.6	25(3)	0.96(06)	$51/2^-$	$47/2^-$	5470
591.5	266(24)	0.99(04)	$39/2^-$	$35/2^-$	3873
593.9	34(4)	0.94(07)	$55/2^-$	$51/2^-$	5865
603.1	7(1)	0.80(15)	$53/2^-$	$51/2^-$	6073
615.6	65(5)	1.05(14)	$51/2^-$	$47/2^-$	4997
621.0	460(40)	1.00(05)	$35/2^-$	$31/2^-$	3281
621.1	14(3)		$(53/2)^-$	$51/2^-$	5618
625.1	5(1)		$(53/2)^-$	$51/2^-$	5897
642.6	64(7)		$37/2^-$	$33/2^-$	3719
658.4	13(2)	0.79(9)	$53/2^-$	$51/2^-$	6028
670.2	20(2)	1.0(3)	$41/2^-$	$37/2^-$	4391
727.7	4(1)			$55/2^-$	6593
736.4	2(1)			$51/2^-$	6008
739.5	9(1)		$43/2^-$	$39/2^-$	4488
742.6	6(1)		$(45/2)^-$	$43/2^-$	5193
762.0	6(2)		$(53/2)^-$	$51/2^-$	5758
770.4	21(5)		$39/2^-$	$35/2^-$	4051
779.8	4(2)		$(59/2)^-$	$57/2^-$	7021
799.0	119(11)	1.15(6)	$43/2^-$	$39/2^-$	4672
809.0	3(1)		$(41/2)^-$	$(39/2)^-$	4889
825.2	10(1)			$41/2^-$	5167
885.4	22(2)		$39/2^-$	$35/2^-$	4167
890.4	102(2)	1.03(5)	$51/2^-$	$47/2^-$	5272
900.3	9(2)		$(53/2)^-$	$51/2^-$	5897
1155.6	2(1)		$(59/2)^-$	$55/2^-$	7021
1287.2	2(1)			$55/2^-$	7153

We turn now to the less aligned $h_{9/2}$ bands with $\alpha = 7/2$ and $\alpha = 5/2$, respectively. As mentioned in Sec. III A, the two levels at 1009 and 1322 keV decaying via 388- and 420-keV transitions into the $11/2^-$ and $15/2^-$ members of the $\alpha = 7/2$ band were proposed in Ref. [15] to constitute the continuation of the $\alpha = 5/2$ sequence built on the $(5/2^-)$ state at 732 keV. In the present work this sequence has been extended up to spin $33/2^-$. Following the prescription presented in Ref. [15], the energy spacings in all three sequences are compared to the ones in the ground-state band of the core nucleus ^{186}Os in Fig. 9. For the $\alpha = 9/2$ and $\alpha = 7/2$ bands the ratios close to unity nicely illustrate their rotation-aligned character. For the proposed $\alpha = 5/2$ band the ratio is clearly lower but shows an increasing trend with increasing angular momentum. However, one should keep in mind that the simple prediction of the rotation-aligned model—that all sequences $I = \alpha, \alpha + 2, \ldots$, with $\alpha \leqslant j$, follow the core excitation energies—is based on the approximation $R \approx I - \alpha$, which applies best to $\alpha = j$ and large values of I. At $I - \alpha = 14\hbar$ the ratio $[E(I - \alpha) - E(I - \alpha - 2)]/[E(R) - E(R - 2)]$ decreases for all three bands. This clearly indicates that the first band crossing observed at a frequency around $\hbar\omega \approx 0.39$ MeV in the yrast bands in ^{187}Ir and ^{186}Os, as discussed previously, takes place at the same frequency in the less aligned $h_{9/2}$ structures too.

B. Multiquasiparticle states

Besides the rotational structures based on the odd proton occupying different single-particle orbitals presented in Fig. 1, a number of three- and even five-quasiparticle states have been observed for the first time in the present work (see Figs. 3 and 7). To study the possible configurations that are expected to be most relevant for the formation of such

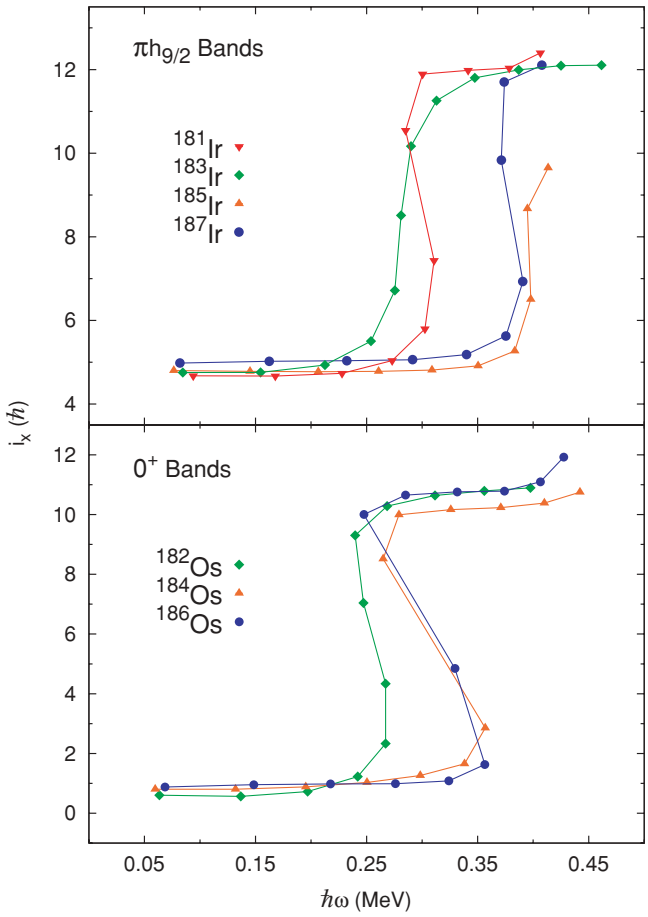

FIG. 8. (Color online) Aligned angular momenta for the $h_{9/2}$ bands in (a) ^{181,183,185,187}Ir and (b) ^{182,184,186}Os. In all cases the excitation energies of a rotor with variable moments of inertia have been subtracted using the Harris parameters $\mathcal{J}_0 = 23.5$ MeV^{-1} $\hbar^2$ and $\mathcal{J}_1 = 75.0$ MeV^{-3} $\hbar^4$ for ^{181}Ir, $\mathcal{J}_0 = 26.8$ MeV^{-1} $\hbar^2$ and $\mathcal{J}_1 = 47.0$ MeV^{-3} $\hbar^4$ for ^{183}Ir, $\mathcal{J}_0 = 27.7$ MeV^{-1} $\hbar^2$ and $\mathcal{J}_1 = 55.0$ MeV^{-3} $\hbar^4$ for ^{185}Ir, $\mathcal{J}_0 = 22.2$ MeV^{-1} $\hbar^2$ and $\mathcal{J}_1 = 65.0$ MeV^{-3} $\hbar^4$ for ^{187}Ir, $\mathcal{J}_0 = 22.2$ MeV^{-1} $\hbar^2$ and $\mathcal{J}_1 = 65.0$ MeV^{-3} $\hbar^4$ for ^{182,184}Os, and $\mathcal{J}_0 = 23.8$ MeV^{-1} $\hbar^2$ and $\mathcal{J}_1 = 55.0$ MeV^{-3} $\hbar^4$ for ^{186}Os.

high-K states, we show in Fig. 10 the single-particle energies in the nucleus ^{186}Os, the even-even core of ^{187}Ir, as a function of the deformation parameter β (taken from Fig. 9 in Ref. [26]). As this figure shows, the most relevant orbitals for generating angular momentum are the intruder orbitals $h_{11/2}$ for protons and $i_{13/2}$ for neutrons. While at intermediate spin (15/2–21/2) a large number of different configurations can contribute to the wave functions, above spin 21/2 at negative parity the wave functions are pure, consisting of a unique configuration. The maximum spin value that can be reached breaking only one pair of nucleons, that is, as a three-quasiparticle state, is $31/2^-$, with two neutrons occupying the $11/2^+[615]$ and $9/2^+[624]$ Nilsson orbitals coupled to the odd $11/2^-[505]$ proton. We assign this maximum-spin three-quasiparticle configuration to the experimentally observed state at an excitation energy of 2755 keV. All configuration assignments proposed in the present work are summarized in Table III. It is interesting to note that the $11/2^+[615] \otimes 9/2^+[624]$ two-neutron con-

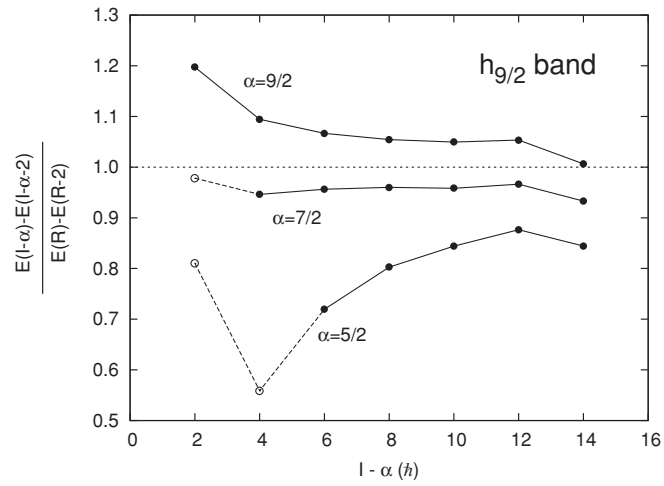

FIG. 9. $\Delta I = 2$ energy differences within the $h_{9/2}$ decoupled bands relative to the corresponding energies in the even-even core nucleus ^{186}Os. States that were identified in Ref. [15] are connected by dashed lines, while levels established in the present work are connected by solid lines.

figuration is observed as $K^\pi = 10^+$ states in both ^{186}Os and ^{188}Os at energies of 2559 and 2564 keV, respectively [19,33]. This $31/2^-$ state at 2755 keV predominantly decays via the 268-keV transition to the isomeric $29/2^-$ level, to which we assign the $\pi\{9/2^-[514]\} \otimes \nu\{11/2^+[615], 9/2^+[624]\}_{K^\pi=10^+}$ configuration.

A possible explanation for the isomerism of this $29/2^-$ state is that the $25/2^-$, 2377-keV and $23/2^-$, 2261-keV levels below involve unpaired neutrons in the negative-parity orbitals $h_{9/2}$ and $f_{7/2}$ rather than in the $i_{13/2}$ shell. We tentatively propose the configurations $\pi 9/2^-[514] \otimes \nu\{9/2^-[505], 7/2^-[503]\}$ and $\pi 11/2^-[505] \otimes \nu\{9/2^-[505], 3/2^-[512]\}$ for these two states (see Table III). While for the $25/2^-$, 2377-keV level, only one decay branch to the $23/2^-$, 2261-keV level has been observed, the latter decays to several $3qp$ states with strongly mixed configurations [$19/2^-$ at 2034 keV, $21/2^-$ at 2226 keV, and $(23/2^-)$ at 2202 keV] as well as to the structure built on the $h_{11/2}$ proton single-particle state. At intermediate spin many different configurations can contribute to the wave functions. For the $19/2^-$ state at 2034 keV, for example, configurations with the odd proton in any of the four single-particle orbitals observed as rotational band heads in this nucleus coupled to a broken neutron pair can contribute as reported in Table III. As a consequence of the strongly mixed character of the state, seven different decay branches to all four $1qp$ structures are observed. Another consequence of the many available configurations at intermediate spin is the existence of a large number of irregular states (see left-hand side of Fig. 3), which, however, cannot be assigned individual configurations.

Besides the $3qp$ states based on unpaired neutrons discussed so far, the formation of three-quasiproton states is also possible in ^{187}Ir. Such pure proton states with a maximum spin of $27/2^-$ have been observed in the odd Au isotopes ^{187,193}Au ($Z = 79$) at excitation energies close to those of the $31/2^-$ maximum-spin states of the $\pi 11/2^-[505] \otimes \nu(i_{13/2})^2$ configuration [27,28]. Because in the Au isotopes the

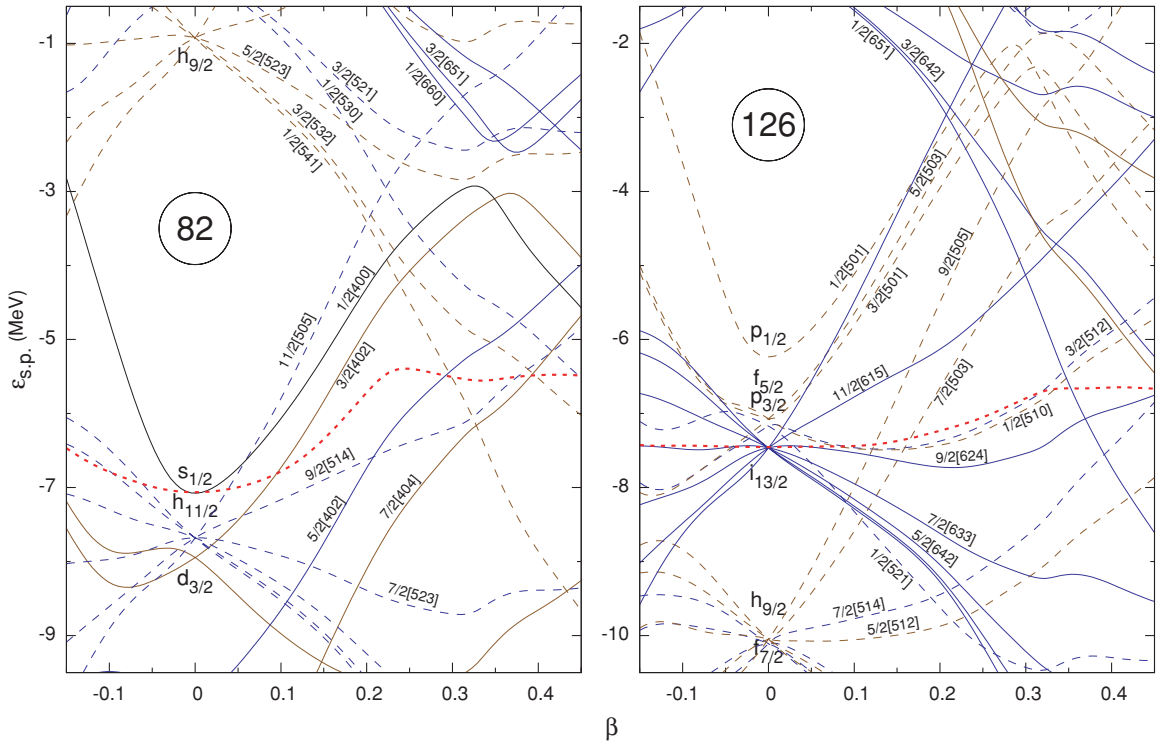

FIG. 10. (Color online) Single-particle energies of the nucleus ^{186}Os, for protons (left) and neutrons (right), as a function of the deformation parameter β. Solid and dashed lines represent positive- and negative-parity orbitals. The dotted (red) lines represent the Fermi level.

$31/2^-$ states decay into these $27/2^-$ states, we suggest that the $27/2^-$ state observed at an excitation energy of 2491 keV in ^{187}Ir and populated via a 264-keV transition from the $31/2^-$, 2755-keV state is of pure proton character. It is interesting to note that this $31/2^- \rightarrow 27/2^-$ transition is isomeric in the Au isotopes, while it is not in ^{187}Ir. The most probable reason for that is that in Au ($Z = 79$) the $\pi 9/2^-[514]$ orbital is farther away from the Fermi level than in Ir ($Z = 77$), and consequently, no $29/2^-$ state with a $\pi 9/2^-[514] \otimes \nu(i_{13/2})^2$ configuration corresponding to the 2487-keV level in ^{187}Ir has

TABLE III. Proposed assignments of multiquasiparticle configurations in ^{187}Ir.

I^π	Proton configuration		Neutron configuration	E_x (keV)
$3/2^+$	$3/2^+[402]$			0
$1/2^+$	$1/2^+[400]$			107
$9/2^-$	$1/2^-[541]$			186
$11/2^-$	$11/2^-[505]$			434
$19/2^-$	$11/2^-[505]$	$\otimes$	$\{7/2^-[503], 1/2^-[510]\}$	2034
	$-1/2^-[541]$	$\otimes$	$\{11/2^+[615], 9/2^+[624]\}$	
	$1/2^+[400]$	$\otimes$	$\{9/2^-[505], 9/2^+[624]\}$	
	$3/2^+[402]$	$\otimes$	$\{7/2^-[503], 9/2^+[624]\}$	
$21/2^-$	$11/2^-[505]$	$\otimes$	$\{9/2^-[505], 1/2^-[510]\}$	2226
	$9/2^-[514]$	$\otimes$	$\{9/2^-[505], 3/2^-[512]\}$	
	$3/2^+[402]$	$\otimes$	$\{9/2^-[505], 9/2^+[624]\}$	
	$1/2^+[400]$	$\otimes$	$\{9/2^-[505], 11/2^+[615]\}$	
$23/2^-$	$11/2^-[505]$	$\otimes$	$\{9/2^-[505], 3/2^-[512]\}$	2261
$25/2^-$	$9/2^-[514]$	$\otimes$	$\{9/2^-[505], 7/2^-[503]\}$	2377
$27/2^-$	$\{11/2^-[505], 9/2^-[514], 7/2^-[523]\}$			2491
$29/2^-$	$9/2^-[514]$	$\otimes$	$\{11/2^+[615], 9/2^+[624]\}$	2487
$31/2^-$	$11/2^-[505]$	$\otimes$	$\{11/2^+[615], 9/2^+[624]\}$	2755
$43/2^-$	$11/2^-[505]$	$\otimes$	$\{11/2^+[615], 9/2^+[624], 9/2^-[505], 3/2^-[512]\}$	4252
$47/2^-$	$11/2^-[505]$	$\otimes$	$\{11/2^+[615], 9/2^+[624], 9/2^-[505], 7/2^-[503]\}$	4381
$47/2^-$	$\{11/2^-[505], 9/2^-[514], 7/2^-[523]\}$	$\otimes$	$\{11/2^+[615], 9/2^+[624]\}$	4896

been observed in the Au isotopes. While the $31/2^-$ state in ^{187}Ir can decay to this $29/2^-$ level just upon movement of the odd proton, this is not the case in Au, leading to a long lifetime of the $31/2^-$ states.

Considering now the level scheme established on top of the $29/2^-$, 2487-keV isomeric state as shown in Fig. 7, one can extend the proposal of configuration assignments even to five-quasiparticle states, although these suggestions have to be considered very preliminary. The $5qp$ configurations that are expected to be lowest in energy are of either $\pi(h_{9/2}) \otimes \nu(i_{13/2}, h_{9/2}, p_{3/2})^4$ or $\pi(h_{9/2})^3 \otimes \nu(i_{13/2})^2$ character. Based on its exclusive decay to the structure built on the $31/2^-$, $\pi 11/2^-[505] \otimes \nu(i_{13/2})^2$ state, we tentatively propose the $\pi 11/2^-[505] \otimes \nu\{11/2^+[615], 9/2^+[624], 9/2^-[505], 3/2^-[512]\}$ configuration for the $43/2^-$ level at 4252 keV. The $47/2^-$ state at 4381 keV populating the $43/2^-$ level via a 129-keV transition could be of the $\pi 11/2^-[505] \otimes \nu\{11/2^+[615], 9/2^+[624], 9/2^-[505], 7/2^-[503]\}$ type. Finally, the second $47/2^-$ state at 4896 keV, which decays to both of the main sequences in the excitation scheme shown in Fig. 7, could correspond to the $\pi(h_{9/2})^3 \otimes \nu(i_{13/2})^2$ configuration involving both proton and neutron alignments (compare Table III).

C. Coupling between γ vibrations and quasiparticle excitations

The $h_{11/2}$ band in the transitional nucleus ^{187}Ir has long garnered special interest from the theoretical side. Different models have been employed to reproduce its irregular behavior. A triaxial rotor model for odd-A nuclei, thus the coupling of the odd nucleon to a triaxially deformed core, was shown to reproduce the properties of this band in a satisfactory way [18,25]. However, it seems somewhat unsatisfactory to employ this model, which is based on rigid triaxial shapes, when a number of different potential energy surface calculations [19,26,30–33] consistently indicate γ softness of the even-even Os core nuclei but do not provide evidence of rigid triaxiality. An alternative way to describe the irregular $h_{11/2}$ band is the γ-vibrational (GV) model, in which the odd particle is coupled to the γ vibration of a symmetric rotor [14]. In this approach the $11/2^-$, $13/2^-$, $15/2^-$, and $17/2^-$ levels at 434, 764, 1160, and 1591 keV, respectively, are proposed to form the rotational band built on the proton $11/2^-[505]$ orbital, while the $15/2^-$, $17/2^-$, and $19/2^-$ states at 964, 1353, and 1721 keV correspond to the $11/2^-[505]$ proton coupled to the one-phonon quadrupole vibration ($\Delta K = 2$). Finally, the $19/2^-$ and $21/2^-$ states observed in Ref. [15] are proposed to be two-phonon-plus-quasiparticle states with $\Delta K = 4$ by Yamazaki *et al.* [14]. In the extended level scheme presented in Fig. 3, two more states have been identified in all three of the mentioned bands. The full scheme of the quasiparticle-vibration coupling is shown on the left-hand side in Fig. 10. Two arguments have been given in favor of the GV model. The first is related to the excitation energy of the $\Delta K = 4$ band. In the triaxial rotor model it is expected to be four times the excitation energy of the $\Delta K = 2$ band, while in the GV model it should have only twice the excitation energy of the latter, which is much closer to the observation. The second argument concerns the ratio of $B(E2)$ transition strengths between the $19/2^- \rightarrow 15/2^-_2$ and the $19/2^- \rightarrow 15/2^-_1$ transitions. In the triaxial rotor model this ratio is 0.7, while in the GV model the $19/2^- \rightarrow 15/2^-_2$ transition is forbidden owing to the K or phonon selection rule. Our experimental limit for the nonobservation of a 363-keV γ ray from the $19/2^-$ to the $15/2^-_2$ state (which was observed in Ref. [16] but not in Ref. [15]) is about a factor of 5 lower than the 8% of the intensity of the 559-keV, $19/2^- \rightarrow 15/2^-_1$ transition, corresponding to a $B(E2)$ ratio of 0.7. The uncertainty in the correct interpretation of the $h_{11/2}$ structure in ^{187}Ir is also reflected in the ongoing discussion about the character of the low-lying $K^\pi = 4^+$ bands in the even-even Os nuclei (to which the odd proton is coupled in the case of ^{187}Ir). Although they have been studied in great detail from both the experimental and the theoretical viewpoint (see Refs. [11] and [13], and references therein), whether these states are double-γ-phonon excitations, one-phonon hexadecapole vibrations, or even of quasiparticle character has still not been definitely established.

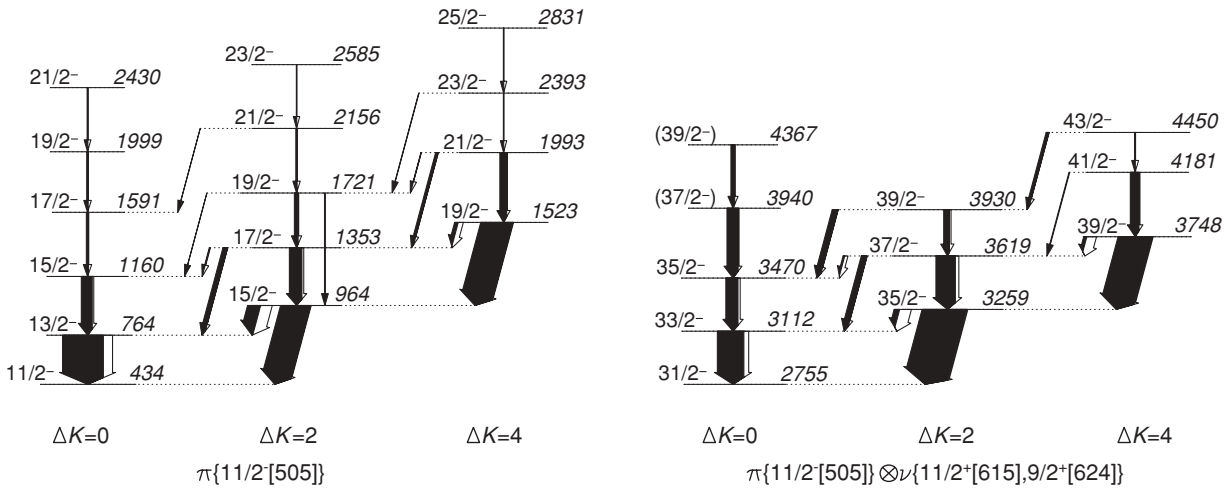

FIG. 11. Band structures based on the $11/2^-$ one-quasiparticle state at 434 keV (left) and the $31/2^-$ three-quasiparticle state at 2755 keV (right).

In the present work, new structures built on top of the $31/2^-$ state at an excitation energy of 2755 keV, with the proposed configuration $\pi\{11/2^-[505]\} \otimes \nu\{11/2^+[615], 9/2^+[624]\}_{K^\pi=10^+}$, have been observed for the first time. Interestingly, these structures very much resemble the ones built on the $11/2^-$ state at 434 keV, as shown in Fig. 11. Again, the excited states can be grouped into three $\Delta I = 1$ sequences, corresponding to states with $K = j$, $K = j + 2$, and $K = j + 4$ or, subtracting the contribution of the odd proton, $\Delta K = 0$, $\Delta K = 2$, and $\Delta K = 4$. In Fig. 11, the bands are shown relative to the respective band head energies, and the similarity between the two structures, with respect to both the excitation energies and the decay patterns, is striking. The ratio between the excitation energies of the $\Delta K = 4$ and $\Delta K = 2$ bands (relative to the $\Delta K = 0$ band) is 2.05 for the structure based on the $11/2^-$ one-quasiparticle state and 1.97 for the structure based on the $31/2^-$ three-quasiparticle level. These values are very close to those found for the $E(4_3^+)/E(2_2^+)$ ratios in ^{188}Os and ^{190}Os, which amount to 2.02 and 2.09, respectively. These observations can be interpreted as robustness of the collective vibrational excitation mode, which hardly changes when either one or even three unpaired nucleons are coupled to it.

V. SUMMARY

The nucleus ^{187}Ir has been populated up to high spin using the reaction ^{186}W(^{7}Li,6n) at a beam energy of 59 MeV. A comprehensive extension of its level scheme has been proposed that comprises 116 newly established excited states connected by 194 γ transitions that have been observed for the first time. All known rotational bands have been extended up to higher spin, and in particular, the band-crossing region of the $h_{9/2}$ band has been revised. A number of new intrinsic high-K states have been identified, and for some of them multiquasiparticle configurations have been tentatively assigned. The three-quasiparticle state with spin $29/2^-$ and an excitation energy of 2487 keV is isomeric, with a half-life of $T_{1/2} = 1.8(5)$ μs. On top of this state, a rich level scheme reaching up to spin $(59/2^-)$ and excitation energies around 7 MeV has been established. Of particular interest is a new structure built on the $31/2^-$, maximum-spin, three-quasiparticle state with the $\pi\{11/2^-[505]\} \otimes \nu\{11/2^+[615], 9/2^+[624]\}$ configuration at 2755 keV. Arguments have been presented indicating a vibrational character of these states similar to the proposed vibration-plus-quasiparticle coupling suggested for the structure built on the $11/2^-$ $h_{11/2}$ proton $1qp$ state.

ACKNOWLEDGMENTS

The authors would like to thank Professor Herbert Hübel, University of Bonn, for providing the ^{186}W target. This work was supported by the Spanish Ministerio de Ciencia e Innovación under Contract Nos. FPA2007-66069 and FPA2009-13377-C02-02 and by the Spanish Consolider-Ingenio 2010 Program CPAN (Grant No. CSD2007-00042).

[1] C. Y. Wu *et al.*, Nucl. Phys. A **607**, 178 (1996).
[2] C. Y. Wu and D. Cline, Phys. Lett. B **382**, 214 (1996).
[3] C. Y. Wu *et al.*, Phys. Rev. C **64**, 014307 (2001).
[4] F. T. Baker, A. Sethi, V. Penumetcha, G. T. Emery, W. P. Jones, M. A. Grimm, and M. L. Whiten, Phys. Rev. C **32**, 2212 (1985).
[5] F. T. Baker *et al.*, Nucl. Phys. A **501**, 546 (1989).
[6] D. G. Burke, M. A. M. Shahabudding, and R. N. Boyd, Phys. Lett. B **78**, 48 (1978).
[7] F. T. Baker *et al.*, Nucl. Phys. A **371**, 68 (1981).
[8] R. D. Bagnell *et al.*, Phys. Lett. B **66**, 129 (1977).
[9] R. D. Bagnell, U. Tanaka, R. K. Sheline, D. G. Burke, and J. D. Sherman, Phys. Rev. C **20**, 42 (1979).
[10] D. G. Burke, Phys. Rev. Lett. **73**, 1899 (1994).
[11] J. M. Allmond, R. Zaballa, A. M Oros-Peusquens, W. D. Kulp, and J. L. Wood, Phys. Rev. C **78**, 014302 (2008).
[12] L. Fortunato, S. De Baerdemacker, and K. Heyde, Phys. Rev. C **74**, 014310 (2006).
[13] N. Lo Iudice and A. V. Sushkov, Phys. Rev. C **78**, 054304 (2008).
[14] T. Yamazaki *et al.*, J. Phys. Soc. Jpn. **44**, 1421 (1978).
[15] P. Kemnitz, L. Funke, H. Sodan, E. Will, and G. Winter, Nucl. Phys. A **245**, 221 (1975).
[16] S. André *et al.*, Nucl. Phys. A **243**, 229 (1975).
[17] J. Meyer ter Vehn, F. S. Stephens, and R. M. Diamond, Phys. Rev. Lett. **32**, 1383 (1974).
[18] J. Meyer ter Vehn, Phys. Lett. B **55**, 273 (1975).
[19] V. Modamio *et al.*, Phys. Rev. C **79**, 024310 (2009).
[20] V. Modamio *et al.* (in preparation, 2010).
[21] C. Séville-Schück *et al.*, Nucl. Phys. A **212**, 45 (1973).
[22] M. Danchev *et al.*, Phys. Rev. C **68**, 054307 (2003).
[23] D. Balabanski *et al.*, Z. Phys. A **332**, 111 (1989).
[24] M. Carpenter *et al.*, Nucl. Phys. A **513**, 125 (1990).
[25] J. Meyer ter Vehn, Nucl. Phys. A **249**, 141 (1975).
[26] A. Jungclaus *et al.*, Phys. Rev. C **77**, 024310 (2008).
[27] J. K. Johansson *et al.*, Phys. Rev. C **40**, 132 (1989).
[28] Y. Gono *et al.*, Nucl. Phys. A **327**, 269 (1979).
[29] N. Perrin *et al.*, Z. Phys. A **359**, 373 (1997).
[30] G. Leander, Nucl. Phys. A **273**, 286 (1976).
[31] C. Wheldon *et al.*, Nucl. Phys. A **699**, 415 (2002).
[32] C. Wheldon, P. M. Walker, P. H. Regan, T. Saitoh, N. Hashimoto, G. Sletten, and F. R. Xu, Phys. Rev. C **59**, R2334 (1999).
[33] C. Wheldon *et al.*, Nucl. Phys. A **652**, 103 (1999).